Ground-state properties of superheavy $Z = 122$ isotopes within the deformed relativistic Hartree-Bogoliubov theory in continuum*

Jin-Hong Zhuang (庄锦泓)[1] Zhen-Hua Zhang (张振华)[1,2†] Yuan-Yuan Wang (王媛媛)[1,2] Cong Pan (潘琮)[3] Kai-Yuan Zhang (张开元)[4] Huan-Yu Zhang (张桓瑜)[1] Yu Sun (孙宇)[1]

[1]Mathematics and Physics Department, North China Electric Power University, Beijing 102206, China
[2]Hebei Key Laboratory of Physics and Energy Technology, North China Electric Power University, Baoding 071000, China
[3]Department of Physics, Anhui Normal University, Wuhu 241000, China
[4]Institute of Nuclear Physics and Chemistry, China Academy of Engineering Physics, Mianyang 621900, China

Abstract: The ground-state properties of superheavy $Z = 122$ isotopes are investigated using the deformed relativistic Hartree-Bogoliubov theory in continuum (DRHBc). Bulk properties, including binding energies, Fermi energies, nucleon separation energies, two-neutron shell gaps, quadrupole deformations, root-mean-square radii, and average pairing gaps, are calculated. The results are compared with those obtained from the relativistic continuum Hartree-Bogoliubov (RCHB) theory. By examining the dependence on the angular-momentum cutoff and the effects of triaxial and octupole deformations, a strategy for determining the ground states is suggested. Furthermore, based on an analysis of the Fermi and nucleon separation energies, the proton and neutron drip lines for $Z = 122$ isotopes are determined within both the DRHBc and RCHB frameworks. The possible magic numbers $N = 184$, 258, and 350 are also suggested. Finally, the evolution of the two-neutron shell gaps, deformation, charge and neutron radii, single-particle levels, and average pairing gaps with increasing neutron number is discussed. These quantities consistently support the suggested neutron shell closure.

Keywords: superheavy nuclei, covariant density functional theory, binding energy, nucleon separation energy, Fermi energy, quadrupole deformation, root-mean-square radius

DOI: 10.1088/1674-1137/ae66d4 **CSTR:** 32044.14.ChinesePhysicsC.50084105

I. INTRODUCTION

The synthesis of new superheavy elements is one of the most important research frontiers in nuclear physics, as it helps us address fundamental questions regarding the boundaries of the nuclear chart and the limits of charge within atomic nuclei. Experimentally, significant progress has been made in the synthesis of superheavy elements. To date, those with atomic numbers $Z \leq 118$ have been synthesized through cold and hot fusion reactions [1−8]. Currently, the synthesis of even heavier new superheavy elements, specifically in the range of $Z = 119$–122, represents a highly competitive frontier in nuclear research. Most of these experiments are concentrating on $Z = 119$ and 120. Despite extensive attempts, no experiment has yet succeeded in synthesizing these new elements [9−17].

Understanding the structure of superheavy elements is quite helpful for synthesizing them. Theoretically, extensive investigations have been conducted using various models, such as macroscopic-microscopic models [18−25] and self-consistent mean-field models [26] including non-relativistic [27−31], and relativistic [32−40] density functional theories. As for the superheavy region, there is little experimental information. Therefore, the extrapolation power of these models is very important.

The deformed relativistic Hartree-Bogoliubov theory in continuum (DRHBc) [41−45], which can concurrently take into account pairing correlations, continuum effects, and degrees of freedom in deformation, is one of the most potent models. It can be viewed as the deformed counterpart of the relativistic continuum Hartree-Bogoliubov (RCHB) theory [46−49], and it has demonstrated remarkable ability in the satisfactory description of ground-state properties through powerful explorations. Based on the DRHBc theory, numerous interesting nuclear phenomena have been investigated, such as the halo phenomena [41, 50−62], the shape evolution and shape coexistence

Received 15 February 2026; Accepted 24 April 2026; Accepted manuscript online 25 April 2026

* This work is supported by the National Natural Science Foundation of China (11875027, 12475121, 12205097, 12305125), the National Key Laboratory of Neutron Science and Technology (NST202401016), the Fundamental Research Funds for the Central Universities (2026SL014), and the High-Performance Computing Platform of North China Electric Power University

† E-mail: zhzhang@ncepu.edu.cn

[63−68], the shell evolution [69−72], fission barriers [73], α-decay half-lives [74, 75], the one-proton emission [76, 77], *etc.* In addition, the ground-state properties of those nuclei in the whole nuclear chart have been calculated and the corresponding nuclear mass tables based on the RCHB and DRHBc theories have been established [78−80].

In Ref. [80], the ground-state properties of even-Z nuclei have been calculated systematically up to $Z = 120$, which is predicted to be a proton magic number. As discussed in Ref. [81], the upper limit of the nuclear charge number may extend to $Z = 173$ according to quantum electrodynamics calculations. Therefore, it is essential to extend theoretical investigations beyond $Z = 120$ within the DRHBc framework. The DRHBc Mass Table Collaboration is now working on the whole nuclear chart including the superheavy nuclei with $121 \le Z \le 136$. In this work, we present the calculations for the ground-state properties across the entire $Z = 122$ isotopic chain using the DRHBc theory, including binding energies, Fermi energies, nucleon separation energies, quadrupole deformations, and root-mean-square (rms) radii, etc. Note that IUPAC has already provided a temporary name "Unbibium" and symbol "Ubb" for the element with $Z = 122$ [82].

This paper is organized as follows. Section II provides a brief introduction to the framework of DRHBc theory. The numerical details of the calculations are described in Sec. III. In Sec. IV, we present the ground-state properties of nuclei in the $Z = 122$ isotopic chain obtained from the DRHBc calculations, with corresponding RCHB results included for comparison. Finally, a brief summary is given in Sec. V.

II. THEORETICAL FRAMEWORK

The details of the DRHBc theory can be found in Refs. [43−45, 83]. Here, we briefly present its formalism. The relativistic Hartree-Bogoliubov (RHB) equation reads [84].

$$\begin{pmatrix} h_D - \lambda_\tau & \Delta \\ -\Delta^* & -h_D^* + \lambda_\tau \end{pmatrix} \begin{pmatrix} U_k \\ V_k \end{pmatrix} = E_k \begin{pmatrix} U_k \\ V_k \end{pmatrix}, \tag{1}$$

where λ_τ is the Fermi energy for neutrons or protons ($\tau = n$ or p), and E_k and $(U_k,\ V_k)^T$ are the quasiparticle energy and wave function, respectively. h_D is the Dirac Hamiltonian,

$$h_D(\boldsymbol{r}) = \boldsymbol{\alpha}\cdot\boldsymbol{p} + V(\boldsymbol{r}) + \beta[M + S(\boldsymbol{r})], \tag{2}$$

where M is the nucleon mass, $S(\boldsymbol{r})$ and $V(\boldsymbol{r})$ are the scalar and vector potentials, respectively, and Δ is the pairing potential.

$$\Delta(\boldsymbol{r}_1,\boldsymbol{r}_2) = V^{\rm pp}(\boldsymbol{r}_1,\boldsymbol{r}_2)\,\kappa(\boldsymbol{r}_1,\boldsymbol{r}_2), \tag{3}$$

where κ is the pairing tensor [85], and $V^{\rm pp}$ is the pairing interaction in the particle-particle channel. Here, a density-dependent zero-range pairing force is adopted,

$$V^{\rm pp}(\boldsymbol{r}_1,\boldsymbol{r}_2) = V_0\frac{1}{2}(1-P^\sigma)\,\delta(\boldsymbol{r}_1-\boldsymbol{r}_2)\left(1-\frac{\rho(\boldsymbol{r}_1)}{\rho_{\rm sat}}\right), \tag{4}$$

in which V_0 is the pairing strength, $\rho_{\rm sat} = 0.152\ {\rm fm}^{-3}$ denotes the saturation density of nuclear matter, and $\frac{1}{2}(1-P^\sigma)$ represents the projector for the spin $S = 0$ component in the pairing channel.

In the DRHBc theory, since axial and reflection symmetries are assumed, the pairing tensor, various densities, and potentials are expanded in terms of the Legendre polynomials.

$$f(\boldsymbol{r}) = \sum_\lambda f_\lambda(r)P_\lambda(\cos\theta), \quad \lambda = 0,2,4,\ldots \tag{5}$$

The RHB equations are solved in the Dirac Woods-Saxon (DWS) basis [86, 87], which can provide an equivalent description to coordinate-space solutions and appropriately describe the large spatial extension of weakly bound nuclei.

For an odd-A nucleus, one needs to further take into consideration the blocking effect for the unpaired single proton or neutron [42]. The equal filling approximation is adopted to deal with the blocking effects in the DRHBc theory [45].

III. NUMERICAL DETAILS

In this work, the relativistic density functional PC-PK1 [88] is adopted. The DWS basis is constructed in a box of $R_{\rm box} = 20$ fm, with a mesh of $\Delta r = 0.1$ fm. For the basis space, the angular momentum cutoff is chosen as $J_{\rm max} = 31/2\,\hbar$, and the energy cutoff in the Fermi sea is $E_{\rm cut} = 300$ MeV. The maximum expansion order in Eq. (5) is $\lambda_{\rm max} = 12$, which is sufficient for our study. For the particle-particle channel, the pairing strength $V_0 = -300$ MeV·fm^3 in Eq. (4), and the pairing window is chosen as 100 MeV. The examinations for the above numerical cutoffs and the pairing parameters have been carried out for $Z = 134$ and 135 isotopes [89]. For comparison, the RCHB calculations are also performed for all the $Z = 122$ isotopes considered. The corresponding numerical details can be found in Ref. [78].

To examine the effects of octupole and triaxial degrees of freedom on the potential energy curves (PECs), the calculations with multi-dimensionally constrained covariant density functional theory (MDC-CDFT) are also carried out for ^{384}Ubb as an example. For comprehensive details on the MDC-CDFT framework, see Refs. [90−93]. In these calculations, the density functional PC-PK1 is also adopted. The Dirac equation is solved by an expansion in the axially deformed harmonic oscillator basis with $N_f = 20$ major shells, which is enough for the superheavy nuclei. Pairing correlations are taken into account in the BCS approximation with a finite range separable pairing force [94]. The pairing strength and effective range are taken as $G/G_0 = 1.1$ and $a = 0.644$ fm, with $G_0 = 728$ MeV·fm^3. The pairing strength is obtained by reproducing the odd-even differences in binding energies of the actinides and superheavy nuclei [95−98]. Both in the DRHBc and MDC-CDFT theories, the microscopic center-of-mass correction is considered [99−101].

IV. RESULTS AND DISCUSSION

The nuclei in the $Z = 122$ isotopic chain, with neutron number from $N = 171$ to 352, are calculated by the DRHBc theory. Bulk properties for the ground states, including binding energies, Fermi energies, separation energies, quadrupole deformations, and rms radii, are obtained. The results are also compared with those obtained from the spherical RCHB calculations.

Figure 1 presents the evolution of the PECs for the $Z = 122$ isotopic chain, calculated from $N = 172$ to $N = 352$ using constrained DRHBc calculations at intervals of $\Delta N = 10$. The ground-state deformations from unconstrained calculations are indicated by solid red triangles. These ground states correspond to the global minima on their respective PECs, validating the self-consistency of the DRHBc calculations. Each PEC typically exhibits several local minima. According to Ref. [89], an angular momentum cutoff of $J_{\max} = 31/2\,\hbar$ in the DRHBc theory has been verified as sufficient for nuclei with proton numbers $Z = 122-136$. That study also recommended that with $J_{\max} = 31/2\,\hbar$, only the lowest minimum in the small-deformation region $|\beta_2| < 0.3$ can be reliably identified as the ground state, whereas the lowest minimum at larger deformations $|\beta_2| > 0.3$ should be checked carefully, because the PECs in the large-deformation region vary significantly as $J_{\max}$ increases. In the present work, numerous minima appear at large oblate ($\beta_2 \sim -0.4$ to -0.5) and prolate ($\beta_2 > 0.5$) deformations. It is therefore essential to determine which minimum in each PEC represents the actual ground state.

The nucleus ^{384}Ubb, which exhibits several minima in its PEC, is taken as an example to show the strategy for determining the ground state. Figure 2 shows the PECs of ^{384}Ubb calculated using the DRHBc theory with different angular momentum cutoffs: $J_{\max} = 23/2\,\hbar$ (black solid

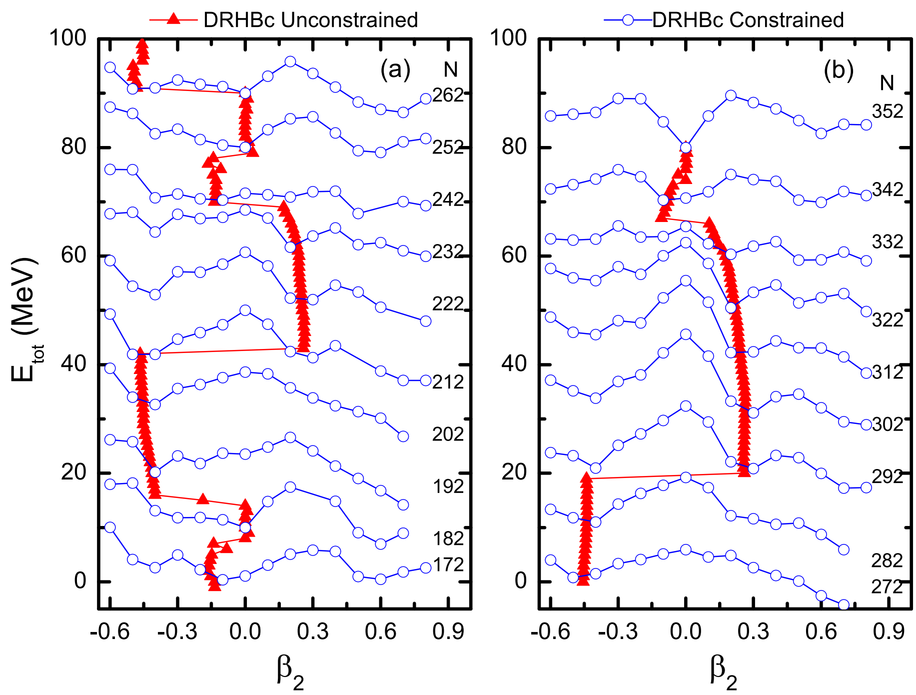

Fig. 1. (color online) The evolution of PECs for the $Z = 122$ isotopic chain as a function of neutron number, from $N = 172$ to $N = 352$, is obtained from constrained DRHBc calculations using the density functional PC-PK1. The calculations are performed at intervals of $\Delta N = 10$. In each panel, the PECs for ^{294}122 ($N = 172$) and ^{394}122 ($N = 272$) are renormalized to the energy of their respective ground states (indicated by red solid triangles). The remaining PECs are successively shifted upward by 1 MeV for each additional neutron. The ground-state deformations determined from unconstrained DRHBc calculations are marked by solid red triangles on the corresponding curves.

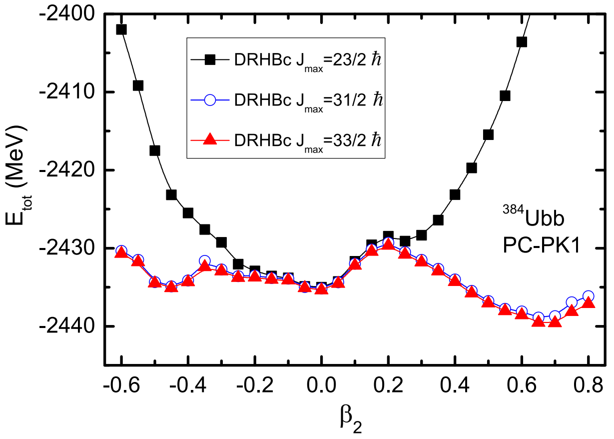

Fig. 2. (color online) The PECs of ^{384}Ubb obtained by the DRHBc calculations are shown with the angular momentum cutoff $J_{max} = 23/2\,\hbar$ (black solid squares), $31/2\,\hbar$ (blue open circles), and $33/2\,\hbar$ (red solid triangles).

squares), $31/2\,\hbar$ (blue open circles), and $33/2\,\hbar$ (red solid triangles). Note that for $J_{max} = 23/2\,\hbar$, the pairing interaction strength is set to $V_0 = -325$ MeV·fm^3 [44]. It can be seen that at $J_{max} = 23/2\,\hbar$, only two minima are present: one spherical minimum and a very shallow prolate minimum around $\beta_2 \sim 0.25$. When J_{max} increases to $31/2\,\hbar$, the PEC drops significantly in both the prolate and oblate large-deformation regions. An obvious oblate minimum appears near $\beta_2 \sim -0.45$, while the prolate minimum shifts to $\beta_2 \sim 0.65$. This behavior is consistent with the findings in Ref. [89] regarding the convergence with respect to J_{max}. In addition, a very flat oblate minimum also appears near $\beta_2 \sim -0.25$. Further increasing J_{max} to $33/2\,\hbar$ leads to nearly converged PECs across most deformation regions, except for the very large prolate deformation ($\beta_2 > 0.6$), which shifts a little (about 0.05). This indicates that an angular momentum cutoff of $J_{max} = 31/2\,\hbar$ is sufficient for the present calculations. Therefore, from the perspective of the axially symmetric and reflection symmetric DRHBc theory, the minimum with large oblate deformation $\beta_2 \sim -0.45$ should be regarded as the ground state, given its lower energy and stability upon further increasing J_{max}. This finding supersedes the previous identification of the minimum within $|\beta_2| < 0.3$ as the ground state [89]. In contrast, whether the lowest minimum with large prolate deformation ($\beta_2 > 0.5$) corresponds to the ground state remains uncertain since it changes slightly with further increasing J_{max}.

It is well known that for actinides and superheavy nuclei, the inner fission barrier is generally lowered when triaxial deformation is allowed, while the outer barrier is further reduced when octupole deformation is considered [73, 102−106]. In some cases, the outer barrier may even disappear after including octupole degrees of freedom. Therefore, it is important to examine whether the minima identified in Fig. 2 remain stable when triaxial and octupole deformations are taken into account. However, the present DRHBc calculations keep both axial and reflection symmetry. Although a triaxial version of the DRHBc theory has recently been developed [107, 108], systematic calculations for superheavy nuclei within this framework remain computationally prohibitive.

The MDC-CDFT developed by Lu *et al.* can break both axial and reflection symmetries [90, 91]. To examine the effects of octupole and triaxial deformations on the energy minima of $Z = 122$ isotopes, we still take ^{384}Ubb as an example and calculate its PECs using MDC-CDFT under different self-consistent symmetry constraints, as shown in Fig. 3. The black solid curve represents the result with axially symmetric and reflection-symmetric (AS-RS) deformation, the red dashed curve corresponds to the axially symmetric but reflection-asymmetric (AS-RA) case, and the olive dash-dotted curve shows the result with triaxial and reflection-symmetric (TA-RS) deformation. Results obtained from the DRHBc calculations are also plotted as blue open circles for comparison. For clarity, the energy at $\beta_2 = 0$ has been subtracted in both the DRHBc and MDC-CDFT calculations. It can be seen that the minima corresponding to spherical, oblate, and prolate deformations are essentially the same between the DRHBc and MDC-CDFT (AS-RS) calculations. The differences arise from the different pairing interactions and basis choices employed in these two methods. When reflection symmetry is broken (AS-RA), the prolate minimum near $\beta_2 \sim 0.7$ disappears. This indicates that an energy minimum exhibiting very large quadrupole deformation should not be identified as the ground state, despite possessing the lowest energy. When axial symmetry is broken (TA-RS), the barrier around $\beta_2 \sim 0.2$ is lowered. Nevertheless, these minima still persist, suggesting that the oblate minimum with $\beta_2 \sim -0.4$ to -0.5 should indeed be considered as the ground state if it possesses the lowest energy. Note that in the calculated PECs for all the $Z = 122$ isotopes, there is no minimum with even larger oblate deformation ($\beta_2 < -0.6$). Whether they can be recognized as ground states when they possess the lowest energy in other isotopes still needs to be checked carefully. Following this strategy, the ground states for all the $Z = 122$ isotopes are determined using the unconstrained DRHBc calculations (red solid triangles in Fig. 1) and the bulk properties, such as binding energies, nucleon separation energies, etc., are obtained.

Figure 4 shows the binding energy per nucleon B/A for the ground states of $Z = 122$ isotopes as a function of neutron number, calculated within both the DRHBc (blue solid line) and the spherical RCHB (red dashed line) frameworks. A local maximum around $N \approx 180$ is observed in the results of both models. This feature is similar to that found for isotopes of $Z = 117-120$ [71], a behavior primarily governed by the competition between the volume energy contribution and the contributions from

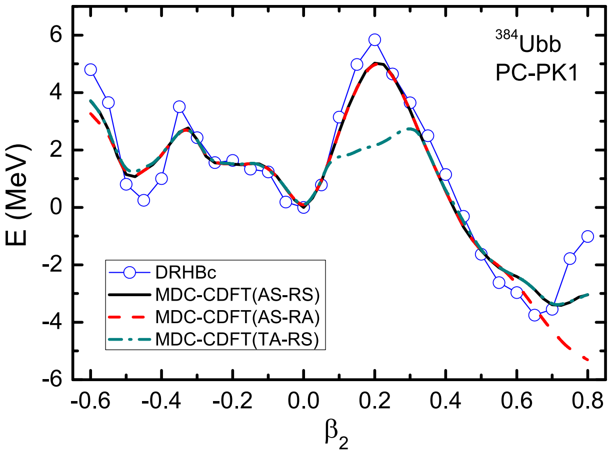

Fig. 3. (color online) The PECs of ^{384}Ubb obtained by the DRHBc theory (blue open circles) and the MDC-CDFT with various self-consistent symmetries imposed are as follows: axially symmetric and reflection symmetric (AS-RS) deformation (black solid curve), axially symmetric and reflection asymmetric (AS-RA) deformation (red dashed curve), and triaxial and reflection symmetric (TA-RS) deformation (olive dash-dotted curve). The energy at $\beta_2 = 0$ is subtracted in the DRHBc and MDC-CDFT calculations, respectively.

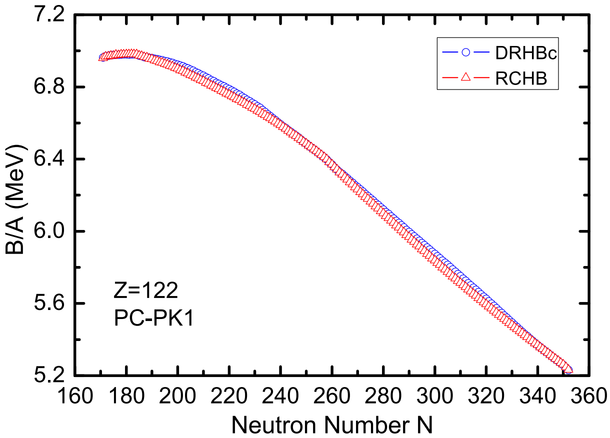

Fig. 4. (color online) The binding energy per nucleon B/A for the ground states of $Z = 122$ isotopes as a function of neutron number is calculated by the DRHBc (blue solid line) and RCHB (red dashed line) theories using the density functional PC-PK1.

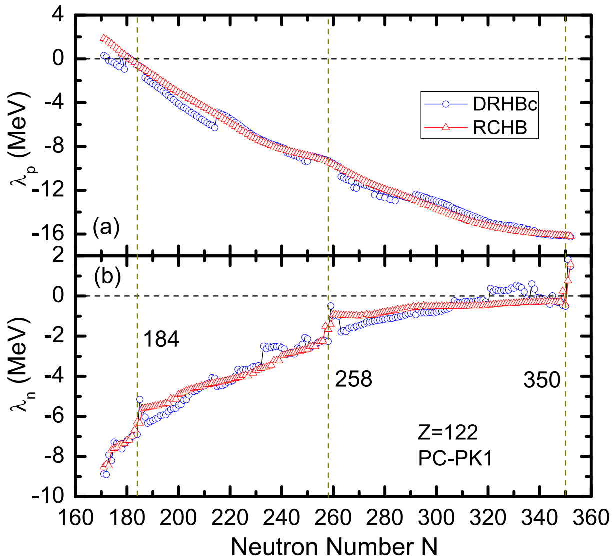

Fig. 5. (color online) The (a) proton Fermi surface λ_p and (b) neutron Fermi surface λ_n for the ground states of $Z = 122$ isotopes as a function of neutron number, calculated by the DRHBc (blue open circles) and the RCHB (red open triangles) theories, using the density functional PC-PK1.

the Coulomb and asymmetry energies. The DRHBc and RCHB results are in close agreement in the neutron-number regions N=171−186, 242−262, and 339−352. This consistency stems from the spherical or weakly oblate deformed shapes of the nuclei in these regions. When deformation is included self-consistently in the DRHBc calculations, the nuclei generally gain additional binding energy compared to the spherical RCHB results.

Figure 5 shows the proton (λ_p) and neutron (λ_n) Fermi energies for the ground states of $Z = 122$ isotopes as a function of neutron number calculated by the DRHBc theory. Results from the spherical RCHB theory are also shown for comparison. As shown in Fig. 5(a), the proton Fermi energy λ_p obtained in the RCHB calculation decreases smoothly with neutron number and becomes negative beyond $N = 181$. We know that the λ_p for the nuclei within the proton drip-line should be negative. However, whether the nucleus is bound also depends on the nucleon separation energies, which are positive for a bound nucleus. From Fig. 6, the two-proton separation energy S_{2p} calculated within RCHB theory is negative for $N \leq 178$. Combining these criteria, the RCHB calculation indicates that ^{303}Ubb ($N = 181$) is the proton drip-line nucleus, with isotopes having $N \leq 180$ being unbound. In the DRHBc results, λ_p shows an overall decreasing trend with neutron number but exhibits abrupt increases at specific neutron numbers. Notably, λ_p first turns negative at $N \geq 173$, then becomes positive again at $N = 180$ and 181. The two-proton separation energy S_{2p} from DRHBc theory (Fig. 6) increases with neutron number, albeit with small fluctuations, and is negative for $N \leq 178$, consistent with the RCHB results. Therefore, according to the DRHBc calculations, isotopes with $N \leq 181$ are unbound, and the proton drip-line nucleus is ^{304}Ubb ($N = 182$).

As for the neutron Fermi energy λ_n [see Fig. 5(b)], it continuously increases with neutron number in both the RCHB and DRHBc calculations, exhibiting sharp rises at specific neutron numbers such as $N = 184$, 258, and 350. These abrupt increases suggest the existence of neutron shell closures. The present calculations identify $N = 184$, 258, and 350 as possible neutron magic numbers, consistent with previous DRHBc studies [109−112]. It can be seen that in the DRHBc results, λ_n becomes positive for

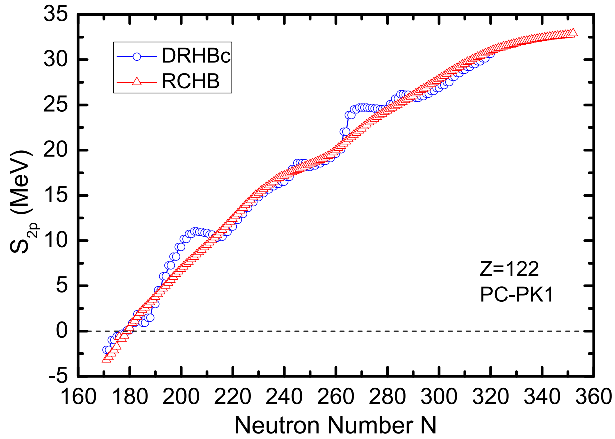

Fig. 6. (color online) The two-proton separation energy S_{2p} for the ground states of $Z = 122$ isotopes as a function of neutron number is calculated by the DRHBc (blue open circles) and the RCHB (red open triangles) theories using the density functional PC-PK1.

$N = 321-334$, turns negative again until $N = 351$, but remains positive for a few nuclei at $N = 337$, 338, and 345. Within the spherical RCHB framework, this phenomenon is less pronounced. The λ_n only becomes positive at $N = 349$ before the shell closure $N = 350$. From Fig. 7(a), it can be seen that the two-neutron separation energy S_{2n} calculated by the DRHBc theory generally decreases with neutron number (with minor fluctuations) and drops sharply precisely at $N = 184$, 258, and 350, which coincide with those sudden increases in the neutron Fermi energy. This correlation confirms $N = 184$, 258, and 350 as neutron magic numbers. The two-neutron separation energy S_{2n} values become negative for $N = 321-340$ and positive again from $N = 341$ to the shell closure $N = 350$, indicating that nuclei with $N = 321-340$ are unbound. This identifies the neutron drip line for $Z = 122$ isotopes in the DRHBc theory as ^{442}Ubb ($N = 320$). However, several nuclei far away from the neutron drip line may still exist. In contrast, the RCHB theory predicts S_{2n} to remain positive until beyond the shell closure $N = 350$, suggesting more bound nuclei than the DRHBc theory. This indicates that treating the deformation effects as well as pairing and continuum effects in a consistent way can significantly affect the predicted location of the neutron drip line [113]. The one-neutron separation energy S_n should also be positive if the nucleus is bound. In Fig. 7(b), it can be seen that S_n also decreases with neutron number and shows sharp drops at the same magic numbers. A clear odd-even staggering is observed in both DRHBc and RCHB calculations. In the DRHBc theory, the S_n for the nuclei at $N = 311$, 313, 315, 317, 341, 343, 345 are negative. This illustrates that several nuclei far away from the neutron drip line $N = 320$ are bound since their Fermi energies are negative, and their one- and two-neutron separation energies are positive. This phenomenon is quite

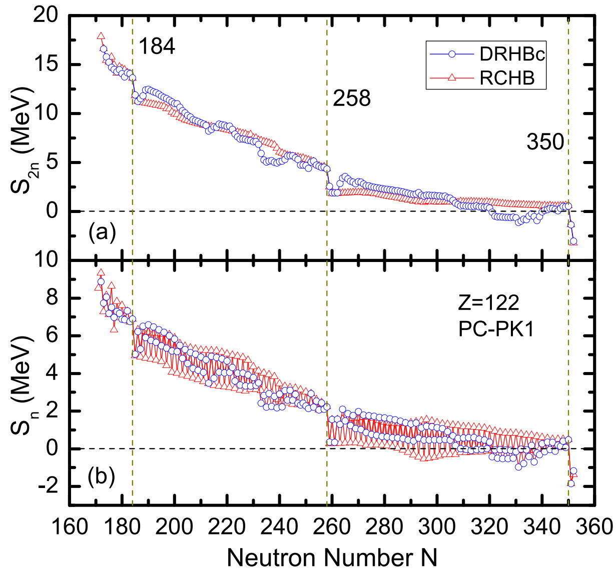

Fig. 7. (color online) The text is identical to Fig. 6, but it now refers to (a) the two-neutron separation energy S_{2n} and (b) the one-neutron separation energy S_n.

similar to the so-called "stability peninsula" identified in the $50 \leq Z \leq 70$ [114] and $100 \leq Z \leq 120$ [115–117] regions. In the RCHB results, S_n is negative for odd-N nuclei in the region $N = 287-341$, marking them as unbound. According to the S_n and S_{2n} systematics in the RCHB theory, the neutron drip line is located at ^{472}Ubb ($N = 350$).

To better illustrate the shell closures and the fine structure of S_{2n} in the $Z = 122$ isotopes, Fig. 8 presents the two-neutron shell gaps, δ_{2n}, as a function of neutron number, calculated using the DRHBc and RCHB theories. δ_{2n} is defined as the difference in S_{2n} between two neighboring nuclei:

$$\delta_{2n}(Z,N) = S_{2n}(Z,N) - S_{2n}(Z,N+2). \tag{6}$$

The overall patterns from the DRHBc and RCHB results are quite similar. At the known or possible shell closures $N = 184$, 258, and 350, both models yield pronounced peaks in δ_{2n}. The DRHBc calculations exhibit more small peaks than the RCHB ones, which can be attributed to deformation effects omitted in the RCHB approach. Most δ_{2n} values from both models are non-negative, reflecting the globally decreasing trend of S_{2n} with increasing neutron number. The DRHBc results show more negative peaks than the RCHB ones. The only two small negative peaks in the RCHB results correspond to nuclei beyond the proton drip line, whereas the negative peaks in the DRHBc results are associated with the fine structure of S_{2n}, indicating shape changes in these isotopes (see Fig. 9). Therefore, it is necessary to examine the evolution of quadrupole deformation in the $Z = 122$

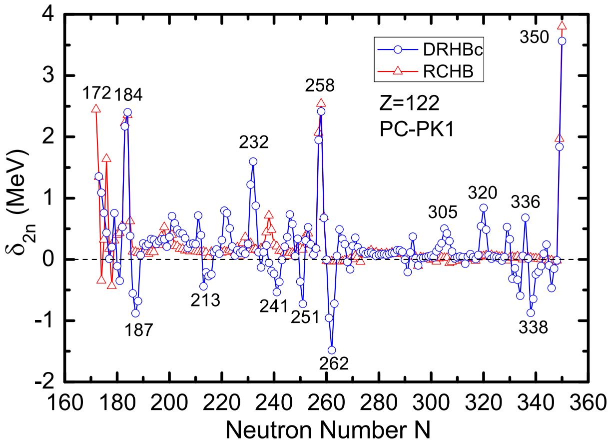

Fig. 8. (color online) Two-neutron shell gaps δ_{2n} for the ground states of $Z = 122$ isotopes as a function of neutron number, calculated by the DRHBc (blue open circles) and the RCHB (red open triangles) theories using the density functional PC-PK1.

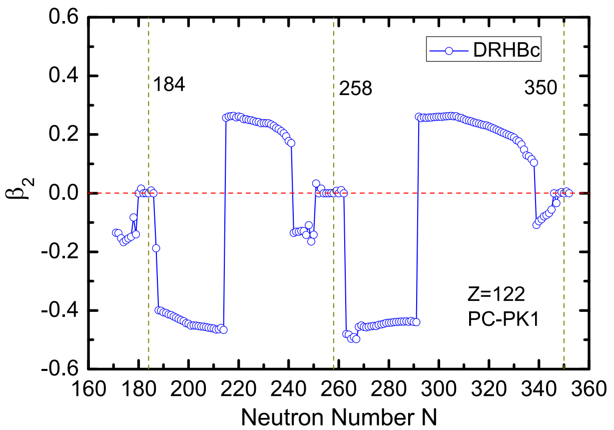

Fig. 9. (color online) The quadrupole deformation β_2 for the ground states of $Z = 122$ isotopes as a function of neutron number is calculated by the DRHBc theory (blue solid circles) using the density functional PC-PK1.

isotopes.

Figure 9 shows the quadrupole deformation β_2 for the ground states of $Z = 122$ isotopes as a function of neutron number calculated by the DRHBc theory. Similar evolutionary patterns can be observed between the predicted magic numbers, specifically in the regions from $N = 184$ to 258 and from $N = 258$ to 350. First, the ground states are spherical or nearly spherical near the magic numbers. Then, with the addition of a few neutrons, they rapidly develop a highly oblate deformation ($\beta_2 \sim -0.4$ to -0.5 in the ranges $N = 188-214$ and $N = 263-291$). Subsequently, the nuclei shift to a moderately prolate deformation ($\beta_2 \sim 0.3$), which then decreases to $\beta_2 \sim 0.1$ as the neutron number increases further. This is followed by a transition to a weakly oblate shape ($\beta_2 \sim -0.1$). Finally, the spherical shape is restored upon approaching the next magic number. It can also be seen that shape transitions occur at $N = 187$, 215, 242, 251, 263, 292, and 339, most of which correspond to or lie near the small peaks in the two-neutron shell gap δ_{2n} shown in Fig. 8.

Figure 10 shows the charge radii ($R_{\rm ch}$) and neutron radii (R_n) for the ground states of $Z = 122$ isotopes as a function of neutron number, calculated by the DRHBc (blue open circles) and the RCHB (red open triangles) theories. For comparison, results from the empirical formula $R_n = r_0 N^{1/3}$ with $r_0 = 1.14$, determined by the neutron rms radius of ^{208}Pb [80], are also shown (dashed line). The empirical formula reproduces the RCHB neutron radii well at smaller neutron numbers, but the deviation grows larger with increasing neutron number. This suggests that isospin-dependent effects become important for accurately describing neutron radii in this region. The $R_{\rm ch}$ and R_n values obtained from the DRHBc and RCHB calculations agree well near the neutron magic numbers $N = 184$, 258, and 350, where the nuclei are spherical in the DRHBc picture. For nuclei with small deformations ($|\beta_2| < 0.3$), the results from the two methods are also quite close. Nearly all DRHBc results are larger than the corresponding RCHB values, except for a few nuclei around $N \sim 340$ with oblate deformation. A similar trend has been observed in earlier DRHBc studies and is attributed to specific shell structures, particularly key single-particle levels near the Fermi surface [118]. For nuclei with large oblate deformation, the DRHBc results are significantly larger than those from the RCHB theory.

Figure 11 displays the single-particle energy levels for spherical configurations of $Z = 122$ isotopes in the ca-

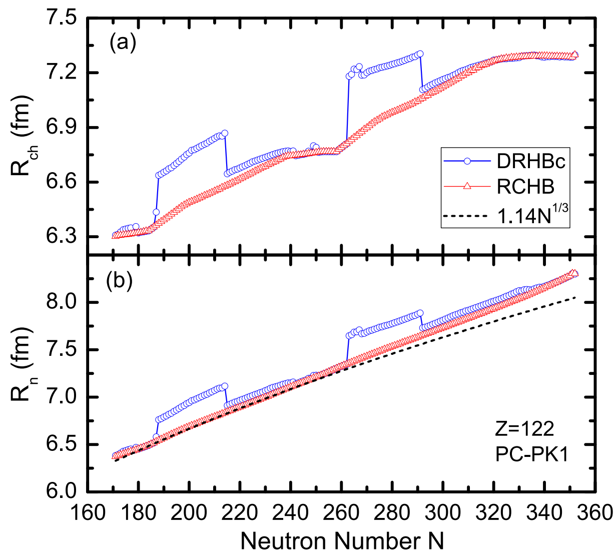

Fig. 10. (color online) (a) The charge radii $R_{\rm ch}$ and (b) the neutron radii R_n for the ground states of $Z = 122$ isotopes as a function of neutron number, calculated by the DRHBc (blue open circles) and the RCHB (red open triangles) theories using the density functional PC-PK1. The results obtained by the empirical formula $R_n = 1.14N^{1/3}$ are shown as a dashed line.

nonical basis as a function of neutron number. The proton levels exhibit relatively smooth evolution with neutron number, except for a limited number of discrete states. Notably, the $Z = 120$ shell gap remains nearly constant across neutron numbers. Due to the intruder orbital $1i_{11/2}$, this gap becomes largest around $N = 258$, which is predicted as a neutron magic number. Additionally, significant spherical shell gaps are observed at $Z = 92$ and $Z = 138$ in Fig. 11(a). The $Z = 92$ shell gap contradicts experimental data and corresponds to a spurious shell closure in certain relativistic mean-field parametrizations [119], though this artifact can be mitigated by density functional updates [120]. The $Z = 138$ shell gap arises from splitting in the proton $3p$ states, where reduced splitting correlates with enhanced gap magnitude. Moreover, there is a relatively smaller spherical shell gap at $Z = 114$ formed by the splitting of proton $2f$ states, and no discernible gap appears at $Z = 126$ in any isotope within the present DRHBc calculations.

For neutron levels in Fig. 11(b), abrupt energy shifts occur for specific orbitals at neutron shell closures $N = 184$, 258, and 350, especially for the positive parity levels. Multiple spherical shell gaps can be identified. The $N = 184$ shell gap diminishes with increasing neutron number owing to the $4s_{1/2}$ state and the intruder state $1j_{13/2}$, whereas the $N = 172$ shell gap remains robust. It weakens significantly only around neutron number $N = 258$. It can be seen that the magnitude of the $N = 172$ shell gap exhibits an inverse correlation with the spin-orbit splitting in $2f$ and $3d$ states: reduced splittings correspond to enhanced gap stability. Similarly, the $N = 258$ shell gap decreases with neutron number due to the $1k_{15/2}$ intruder orbital. It nearly vanishes around the neutron drip line $N = 320$. Note that the $N = 350$ shell gap is not displayed as it resides in the positive energy continuum, where resonant states dominate.

The average pairing gap Δ provides detailed information about the impact of pairing correlations and serves as an important indicator of possible shell closures. Fig. 12 shows the proton pairing gap Δ_p and neutron pairing gap Δ_n for the ground states of even-even $Z = 122$ isotopes as a function of neutron number, as calculated by DRHBc theory. The neutron pairing gap Δ_n drops to zero at the candidate shell closures $N = 184$, 258, and 350, as well as at specific neutron numbers such as $N = 232$, 320, 336, and 344, which may correspond to subshell closures. In addition, Δ_n also shows decreases (not to zero) at several positions. Note that these subshell structures are not discernible in Fig. 11(b) due to either their origin in deformed shell gaps or their location within the positive energy region. Between the shell and subshell closures, Δ_n first increases and then decreases, exhibiting arch-like structures. The average pairing gap also reflects nuclear deformation, as the mean field is influenced by pairing correlations. Since $Z = 120$ is a magic number [see Fig. 11(a)] predicted by the covariant density functional theory [26], proton pairing collapse may still occur when two more protons are added for the $Z = 122$ isotopes. The

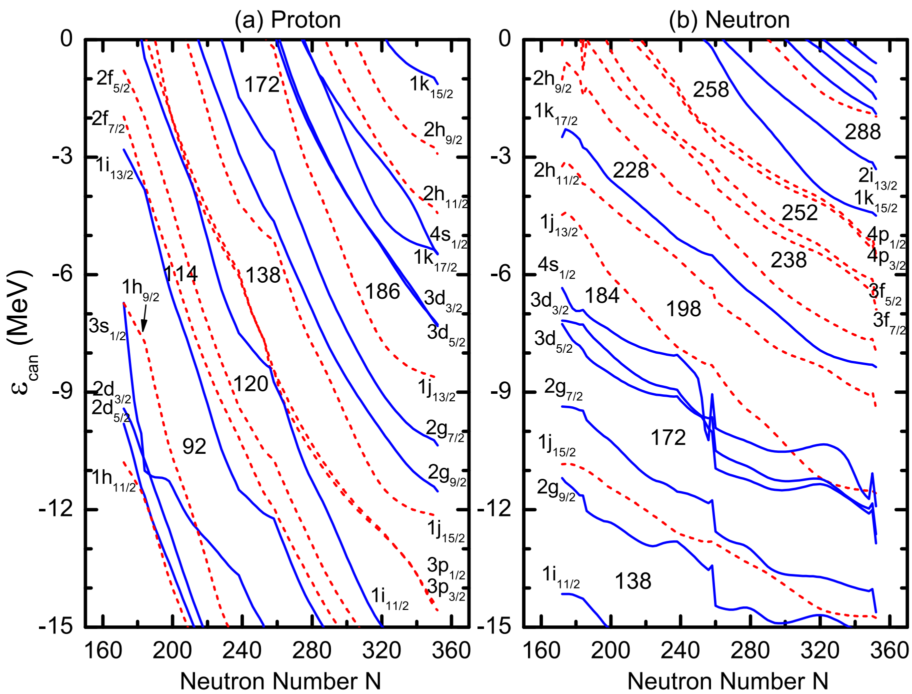

Fig. 11. (color online) Single-particle energy levels for spherical states of $Z = 122$ isotopes are shown separately for (a) protons and (b) neutrons in the canonical basis as a function of neutron number. The positive and negative parity levels are denoted by blue solid and red dashed lines, respectively.

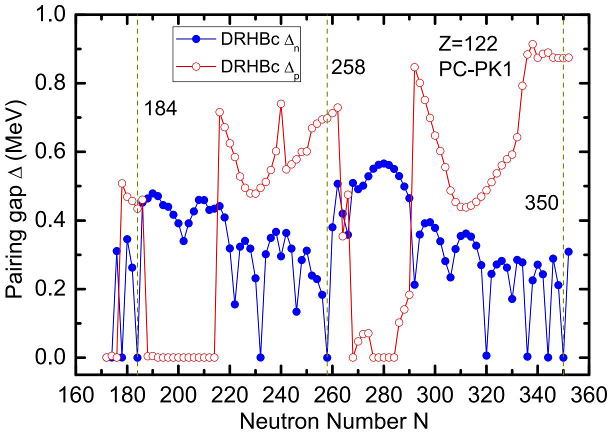

Fig. 12. (color online) The proton and neutron pairing gaps, Δ_p (red open circles) and Δ_n (blue solid circles), for the ground states of even-even $Z = 122$ isotopes as a function of neutron number, are calculated by DRHBc theory using the density functional PC-PK1.

proton pairing gap Δ_p becomes zero or very small in several mass regions. Interestingly, these regions coincide exactly with those where the nuclei exhibit large oblate deformations (see Fig. 9). In regions where Δ_p is relatively larger, it first decreases and then increases, exhibiting inverted arch-like structures that contrast with the behavior of Δ_n. As can be seen in Fig. 9, the nuclei in these regions are all prolate deformed, weakly oblate deformed, or spherical.

V. SUMMARY

In this work, the ground-state properties of superheavy $Z = 122$ isotopes are investigated using the deformed relativistic Hartree-Bogoliubov theory in continuum. Bulk properties of the ground states, including binding energies, Fermi energies, nucleon separation energies, quadrupole deformations β_2, two-neutron shell gaps δ_{2n}, root-mean-square radii, and average pairing gaps, are calculated. The results are also compared with those obtained from the spherical relativistic continuum Hartree-Bogoliubov theory. By examining the effects of angular momentum cutoff $J_{\max}$, triaxial deformation, and octupole deformation, a strategy for determining the ground states is proposed. The present investigation shows that an angular momentum cutoff of $J_{\max} = 31/2\,\hbar$ is sufficient for the $Z = 122$ isotopes. The inclusion of octupole deformation eliminates the large prolate minimum, while triaxial deformation only lowers the first barrier on the prolate side, leaving the minima in the potential energy curve unchanged. Furthermore, based on an analysis of Fermi and separation energies, the proton and neutron drip lines for $Z = 122$ isotopes are determined within both the DRHBc and RCHB frameworks. Possible neutron magic numbers at $N = 184$, 258, and 350 are also suggested. Finally, the evolution of the two-neutron shell gaps, deformation, charge and neutron radii, single-particle levels, and average pairing gaps with increasing neutron number is discussed. These quantities consistently support the suggested neutron shell closure.

ACKNOWLEDGEMENTS

Helpful discussions with members of the DRHBc Mass Table Collaboration are gratefully acknowledged.

References

[1] S. Hofmann and G. Münzenberg, Rev. Mod. Phys. **72**, 733 (2000)
[2] K. Morita, K. Morimoto, D. Kaji *et al.*, J. Phys. Soc. Jpn. **73**, 2593 (2004)
[3] Y. Oganessian, J. Phys. G: Nucl. Part. Phys. **34**, R165 (2007)
[4] Y. T. Oganessian, F. S. Abdullin, P. D. Bailey *et al.*, Phys. Rev. Lett. **104**, 142502 (2010)
[5] S. G. Zhou, Physics **43**, 817 (2014)
[6] S. G. Zhou, Nucl. Phys. Rev. **34**, 318 (2017)
[7] Y. M. Jiang, D. D. Zhang, and S. G. Zhou, Physics **54**, 599 (2025)
[8] X. Y. Huang, Z. Y. Zhang, J. G. Wang *et al.*, Chin. Phys. Lett. **43**, 010101 (2025)
[9] Y. T. Oganessian, V. K. Utyonkov, Y. V. Lobanov *et al.*, Phys. Rev. C **79**, 024603 (2009)
[10] S. Hofmann, S. Heinz, R. Mann *et al.*, Eur. Phys. J. A **52**, 116 (2016)
[11] S. Hofmann, S. Heinz, R. Mann *et al.*, Eur. Phys. J. A **52**, 180 (2016)
[12] J. Khuyagbaatar, A. Yakushev, C. E. Düllmann *et al.*, Phys. Rev. C **102**, 064602 (2020)
[13] H. Sakai, H. Haba, K. Morimoto *et al.*, Eur. Phys. J. A **58**, 238 (2022)
[14] M. Tanaka, P. Brionnet, M. Du *et al.*, J. Phys. Soc. Jpn. **91**, 084201 (2022)
[15] Z. G. Gan, W. X. Huang, Z. Y. Zhang *et al.*, Eur. Phys. J. A **58**, 158 (2022)
[16] J. M. Gates, R. Orford, D. Rudolph *et al.*, Phys. Rev. Lett. **133**, 172502 (2024)
[17] M.-H. Zhang, Z.-Y. Zhang, Z.-G. Gan *et al.*, Nucl. Sci. Tech. **36**, 204 (2025)
[18] A. Sobiczewski, F. Gareev, and B. Kalinkin, Phys. Lett. **22**, 500 (1966)
[19] H. Meldner, Ark. Fys. **36**, 593 (1966)
[20] S. G. Nilsson, J. R. Nix, A. Sobiczewski *et al.*, Nucl. Phys. A **115**, 545 (1968)
[21] S. G. Nilsson, C. F. Tsang, A. Sobiczewski *et al.*, Nucl. Phys. A **131**, 1 (1969)
[22] U. Mosel and W. Greiner, Z. Phys. A **222**, 261 (1969)
[23] P. Möller and J. R. Nix, J. Phys. G: Nucl. Part. Phys. **20**, 1681 (1994)
[24] Q. Mo, M. Liu, and N. Wang, Phys. Rev. C **90**, 024320 (2014)

[25] N. Wang, M. Liu, X. Wu, and J. Meng, Phys. Lett. B **734**, 215 (2014)
[26] M. Bender, P.-H. Heenen, and P.-G. Reinhard, Rev. Mod. Phys. **75**, 121 (2003)
[27] S. Ćwiok, S. Hofmann, and W. Nazarewicz, Nucl. Phys. A **573**, 356 (1994)
[28] S. Ćwiok, J. Dobaczewski, P. H. Heenen *et al.*, Nucl. Phys. A **611**, 211 (1996)
[29] S. Ćwiok, W. Nazarewicz, and P. H. Heenen, Phys. Rev. Lett. **83**, 1108 (1999)
[30] S. Ćwiok, P.-H. Heenen, and W. Nazarewicz, Nature **433**, 705 (2005)
[31] L. M. Robledo, T. R. Rodríguez, and R. R. Rodríguez-Guzmán, J. Phys. G: Nucl. Part. Phys. **46**, 013001 (2018)
[32] G. A. Lalazissis, M. M. Sharma, P. Ring *et al.*, Nucl. Phys. A **608**, 202 (1996)
[33] W. Zhang, J. Meng, S. Zhang *et al.*, Nucl. Phys. A **753**, 106 (2005)
[34] A. V. Afanasjev, T. L. Khoo, S. Frauendorf *et al.*, Phys. Rev. C **67**, 024309 (2003)
[35] J. J. Li, W. H. Long, J. Margueron *et al.*, Phys. Lett. B **732**, 169 (2014)
[36] S. E. Agbemava, A. V. Afanasjev, T. Nakatsukasa *et al.*, Phys. Rev. C **92**, 054310 (2015)
[37] A. V. Afanasjev, S. E. Agbemava, and A. Gyawali, Phys. Lett. B **782**, 533 (2018)
[38] S. E. Agbemava, A. V. Afanasjev, A. Taninah *et al.*, Phys. Rev. C **99**, 034316 (2019)
[39] S. E. Agbemava and A. V. Afanasjev, Phys. Rev. C **103**, 034323 (2021)
[40] A. Taninah, S. E. Agbemava, and A. V. Afanasjev, Phys. Rev. C **102**, 054330 (2020)
[41] S.-G. Zhou, J. Meng, P. Ring *et al.*, Phys. Rev. C **82**, 011301R (2010)
[42] L.-L. Li, J. Meng, P. Ring *et al.*, Chin. Phys. Lett. **29**, 042101 (2012)
[43] L. Li, J. Meng, P. Ring, E.-G. Zhao, and S.-G. Zhou, Phys. Rev. C **85**, 024312 (2012)
[44] K. Zhang, M.-K. Cheoun, Y.-B. Choi *et al.*(DRHBc Mass Table Collaboration), Phys. Rev. C **102**, 024314 (2020)
[45] C. Pan, M.-K. Cheoun, Y.-B. Choi *et al.* (DRHBc Mass Table Collaboration), Phys. Rev. C **106**, 014316 (2022)
[46] J. Meng and P. Ring, Phys. Rev. Lett. **80**, 460 (1998)
[47] J. Meng and P. Ring, Phys. Rev. Lett. **77**, 3963 (1996)
[48] J. Meng, Nucl. Phys. A **635**, 3 (1998)
[49] J. Meng, H. Toki, S. Zhou *et al.*, Prog. Part. Nucl. Phys. **57**, 470 (2006)
[50] J. Meng and S. G. Zhou, J. Phys. G: Nucl. Part. Phys. **42**, 093101 (2015)
[51] X.-X. Sun, J. Zhao, and S.-G. Zhou, Phys. Lett. B **785**, 530 (2018)
[52] X.-X. Sun, J. Zhao, and S.-G. Zhou, Nucl. Phys. A **1003**, 122011 (2020)
[53] X.-X. Sun, Phys. Rev. C **103**, 054315 (2021)
[54] X.-X. Sun and S.-G. Zhou, Sci. Bulletin **66**, 2072 (2021)
[55] S.-Y. Zhong, S.-S. Zhang, X.-X. Sun *et al.*, Sci. China-Phys. Mech. Astron. **65**, 262011 (2022)
[56] K. Y. Zhang, S. Q. Yang, J. L. An *et al.*, Phys. Lett. B **844**, 138112 (2023)
[57] L.-Y. Wang, K. Zhang, J.-L. An *et al.*, Eur. Phys. J. A **60**, 251 (2024)
[58] K. Y. Zhang, C. Pan, and S. Wang, Phys. Rev. C **110**, 014320 (2024)
[59] C. Pan, K. Zhang, and S. Zhang, Phys. Lett. B **855**, 138792 (2024)
[60] J.-L. An, K.-Y. Zhang, Q. Lu *et al.*, Phys. Lett. B **849**, 138422 (2024)
[61] K. Y. Zhang and X. X. Lu, Phys. Lett. B **871**, 139989 (2025)
[62] P. Papakonstantinou, M. Mun, C. Pan *et al.*, Phys. Rev. C **112**, 044301 (2025)
[63] S. Kim, M.-H. Mun, M.-K. Cheoun *et al.*, Phys. Rev. C **105**, 034340 (2022)
[64] Y.-B. Choi, C.-H. Lee, M.-H. Mun *et al.*, Phys. Rev. C **105**, 024306 (2022)
[65] P. Guo, C. Pan, Y. C. Zhao *et al.*, Phys. Rev. C **108**, 014319 (2023)
[66] X. Y. Zhang, Z. M. Niu, W. Sun *et al.*, Phys. Rev. C **108**, 024310 (2023)
[67] M.-H. Mun, E. Ha, Y.-B. Choi *et al.*, Phys. Rev. C **110**, 024310 (2024)
[68] M.-H. Mun, P. Papakonstantinou, and Y. Kim, Particles **8**, 32 (2025)
[69] K. Y. Zhang, P. Papakonstantinou, M.-H. Mun *et al.*, Phys. Rev. C **107**, L041303 (2023)
[70] R.-Y. Zheng, X.-X. Sun, G.-F. Shen *et al.*, Chin. Phys. C **48**, 014107 (2024)
[71] Y. X. Zhang, B. R. Liu, K. Y. Zhang *et al.*, Phys. Rev. C **110**, 024302 (2024)
[72] Z.-D. Huang, W. Zhang, S.-Q. Zhang *et al.*, Phys. Rev. C **111**, 034314 (2025)
[73] W. Zhang, J.-K. Huang, T.-T. Sun *et al.*, Chin. Phys. C **48**, 104105 (2024)
[74] Y.-B. Choi, C.-H. Lee, M.-H. Mun *et al.*, Phys. Rev. C **109**, 054310 (2024)
[75] M.-H. Mun, K. Heo, and M.-K. Cheoun, Particles **8**, 42 (2025)
[76] Y. Xiao, S.-Z. Xu, R.-Y. Zheng *et al.*, Phys. Lett. B **845**, 138160 (2023)
[77] Q. Lu, K.-Y. Zhang, and S.-S. Zhang, Phys. Lett. B **856**, 138922 (2024)
[78] X. W. Xia, Y. Lim, P. W. Zhao *et al.*, At. Data Nucl. Data Tables **121-122**, 1 (2018)
[79] K. Zhang, M.-K. Cheoun, Y.-B. Choi *et al.*, At. Data Nucl. Data Tables **144**, 101488 (2022)
[80] P. Guo, X. Cao, K. Chen *et al.*, At. Data Nucl. Data Tables **158**, 101661 (2024)
[81] P. Indelicato and A. Karpov, Nature **498**, 40 (2013)
[82] J. Chatt, Pure & Appl. Chem. **51**, 381 (1979)
[83] Y. Chen, L. Li, H. Liang *et al.*, Phys. Rev. C **85**, 067301 (2012)
[84] H. Kucharek and P. Ring, Z. Phys. A **339**, 23 (1991)
[85] P. Ring and P. Schuck, *The Nuclear Many-Body Problem* (Springer-Verlag, 1980)
[86] S.-G. Zhou, J. Meng, and P. Ring, Phys. Rev. C **68**, 034323 (2003)
[87] K. Y. Zhang, C. Pan, and S. Q. Zhang, Phys. Rev. C **106**, 024302 (2022)
[88] P. W. Zhao, Z. P. Li, J. M. Yao *et al.*, Phys. Rev. C **82**, 054319 (2010)
[89] S. Wang, P. Guo, and C. Pan, Particles **7**, 1139 (2024)
[90] B.-N. Lu, E.-G. Zhao, and S.-G. Zhou, Phys. Rev. C **85**, 011301R (2012)
[91] B.-N. Lu, J. Zhao, E.-G. Zhao *et al.*, Phys. Rev. C **89**, 014323 (2014)
[92] S.-G. Zhou, Phys. Scr. **91**, 063008 (2016)

[93] J. Zhao, B.-N. Lu, E.-G. Zhao *et al*., Phys. Rev. C **95**, 014320 (2017)
[94] Y. Tian, Z. Ma, and P. Ring, Phys. Lett. B **676**, 44 (2009)
[95] J. Zhao, B.-N. Lu, D. Vretenar *et al*., Phys. Rev. C **91**, 014321 (2015)
[96] X. Meng, B.-N. Lu, and S.-G. Zhou, Sci. China-Phys. Mech. Astron. **63**, 212011 (2020)
[97] X.-Q. Wang, X.-X. Sun, and S.-G. Zhou, Chin. Phys. C **46**, 024107 (2021)
[98] X.-Q. Deng and S.-G. Zhou, Int. J. Mod. Phys. E **32**, 2340004 (2023)
[99] M. Bender, K. Rutz, P.-G. Reinhard *et al*., Eur. Phys. J. A **7**, 467 (2000)
[100] W. Long, J. Meng, N. V. Giai *et al*., Phys. Rev. C **69**, 034319 (2004)
[101] P.-W. Zhao, B.-Y. Sun, and J. Meng, Chin. Phys. Lett. **26**, 112102 (2009)
[102] J. Damgaard, H. C. Pauli, V. V. Pashkevich *et al*., Nucl. Phys. A **135**, 432 (1969)
[103] P. Möller and S. G. Nilsson, Phys. Lett. B **31**, 283 (1970)
[104] M. Girod and B. Grammaticos, Phys. Rev. C **27**, 2317 (1983)
[105] K. Rutz, J. Maruhn, P.-G. Reinhard *et al*., Nucl. Phys. A **590**, 680 (1995)
[106] H. Abusara, A. V. Afanasjev, and P. Ring, Phys. Rev. C **82**, 044303 (2010)
[107] K. Y. Zhang, S. Q. Zhang, and J. Meng, Phys. Rev. C **108**, L041301 (2023)
[108] K. Y. Zhang, S. Q. Zhang, and J. Meng, Phys. Rev. C **112**, 044308 (2025)
[109] P. Du and J. Li, Particles **7**, 1086 (2024)
[110] W.-J. Liu, C.-J. Lv, P. Guo *et al*., Particles **7**, 1078 (2024)
[111] C. Pan and X.-H. Wu, Particles **8**, 2 (2025)
[112] L. Wu, W. Zhang, J. Peng *et al*., Particles **8**, 19 (2025)
[113] E. J. In, P. Papakonstantinou, Y. Kim *et al*., Int. J. Mod. Phys. E **30**, 2150009 (2021)
[114] C. Pan, K. Y. Zhang, P. S. Chong *et al*., Phys. Rev. C **104**, 024331 (2021)
[115] K. Zhang, X. He, J. Meng *et al*., Phys. Rev. C **104**, L021301 (2021)
[116] X.-T. He, C. Wang, K.-Y. Zhang *et al*., Chin. Phys. C **45**, 101001 (2021)
[117] X.-T. He, J.-W. Wu, K.-Y. Zhang *et al*., Phys. Rev. C **110**, 014301 (2024)
[118] C. Pan and J. Meng, Phys. Rev. C **112**, 024316 (2025)
[119] K. Rutz, M. Bender, P.-G. Reinhard *et al*., Nucl. Phys. A **634**, 67 (1998)
[120] W. Long, H. Sagawa, N. V. Giai *et al*., Phys. Rev. C **76**, 034314 (2007)